Journal of Computer Assisted Tomography
4(3):351–360, June

Plastic Scintillation Detectors for High Resolution Emission Computed Tomography

John A. McIntyre

Abstract: The cost of ring tomographs increases rapidly when spatial resolution is improved to 2 mm and better. However, increased cost can be largely avoided by coding the light transmitted from the individual scintillators to the photomultipliers. Unfortunately, there is a factor-of-100 light loss associated with the coding; this loss destroys the pulse height resolution of the pulse spectrum. In addition, the light loss increases the coincidence time resolution of the photomultiplier pulses for inorganic scintillators such as bismuth germanate (BGO). The time resolution can be regained by using plastic scintillators (NE102), and it is shown that the pulse height resolution is unnecessary for cameras with 2 mm resolution. Furthermore, when considering millimeter-sized detectors, (1) detector rings of multiple plastic scintillators can have as good a detection efficiency as BGO, (2) light can be extracted from multiple-scintillator arrays using optical coding methods, (3) cross-talk between plastic scintillators is much smaller than for BGO scintillators, (4) even with the factor-of-100 light loss introduced by the optical coding, the scintillation detection efficiency is about 80% with NE102, (5) an argument is presented that the time required to obtain statistically useful data varies only as the square of the pixel dimension (rather than as the fifth power), and (6) by using multiple ring tomographs there is no loss in sensitivity for pixel sizes down to 2 mm. Optical coding with plastic scintillators appears, then, to make technically practical the construction of ring tomographs with spatial resolutions of 2 mm. Index Terms: Emission computed tomography—Positron emission tomography—Plastic scintillation detectors—High resolution—Detectors.

Recently, Cho and Farukhi (1) suggested that bismuth germanate (BGO) be used as the scintillation detector in positron tomographs. Derenzo (2) has also investigated the utility of BGO and has listed its advantages. Furthermore, Derenzo et al. (3) have tested BGO in their 280-scintillator detector ring and have decided to replace their NaI(Tl) scintillators with BGO. Also, Thompson et al. (4) have installed BGO scintillators in their ring tomograph, while Cho et al. (5) have made further measurements with BGO scintillators for use in a proposed ring tomograph. Thus there appears to be a consensus at this time that BGO is the scintillator of choice for positron ring cameras, although Ter-Pogossian et al. are constructing a small tomograph using NaI(Tl) scintillators (6).

The purpose of this paper is to present arguments for using plastic scintillators in ring tomographs designed for improved spatial resolution. The arguments will be presented in brief form here; details of a tomograph design (7) and of the novel light transmission system (8) will be presented elsewhere. For convenience of reference, the notation and specifications of the tomograph designed at the Donner Laboratory (9) will be used as much as possible.

From the Physics Department, Texas A&M University, College Station, Texas 77843.

A. TOMOGRAPH DESIGN

The schematic drawing in Fig. 1 shows a positron ring tomograph. There are 10 detector rings (only 4 are shown), the rings being separated by lead shields which extend a distance T_0 beyond the detectors toward the center of the ring. An open diameter of 50 cm is provided inside this shielding for the patient, whose body contains the positron-emitting material.

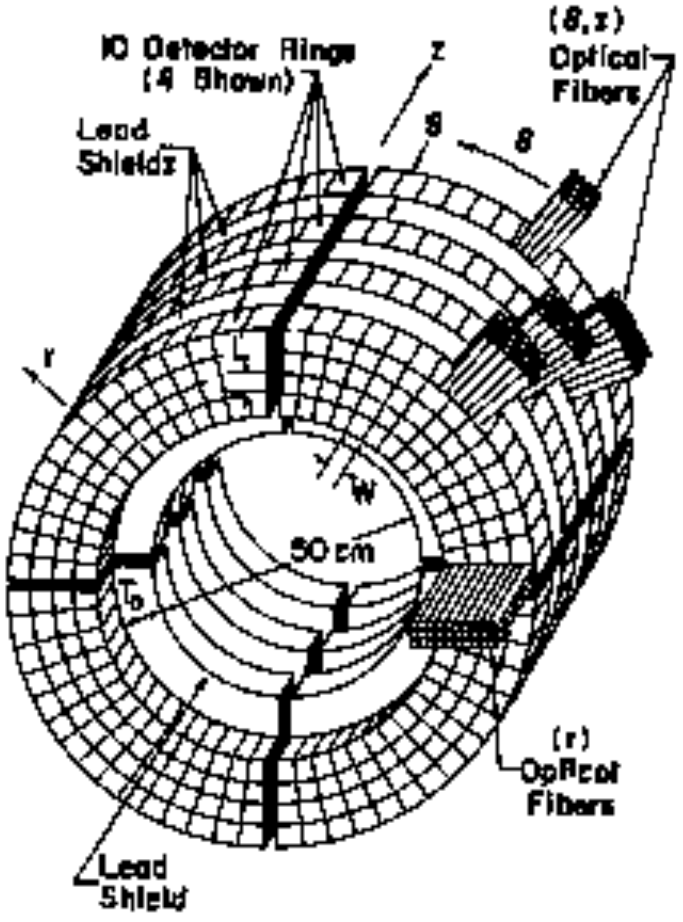

FIG. 1. Schematic drawing of positron ring tomograph.

1. Spatial Resolution and Sampling

The spatial resolution of an image produced by a positron tomograph is limited ultimately by (a) the range of the positrons emitted by the radioactive source (10) and (b) the deviation from 180° of the angle between the annihilation gamma rays (11). For a detector ring with a radius in the neighborhood of 40 cm, the full-width half-maximum (FWHM) spread of a point positron source is found to be in the 2 mm range [7].

The spatial resolution of the tomograph, then, should be about 2 mm, and preferably less, if the maximum possible detail is to be obtained of the positron source distribution.

As shown by Brooks et al. [12], the scintillator "widths" in the ring tomograph should be, at most, twice the spatial resolution desired for the tomograph. Choosing a value of 2 mm for the *largest* desired value for the resolution, the scintillator "width" is selected to be 4 mm, and the sampling interval required is 1 mm.

A stationary ring tomograph with 4 mm scintillators will provide only 4 mm sampling. The scintillators are actually made 2 mm wide and electronically grouped in pairs. By changing the combinations of pairs the sampling interval is reduced to 2 mm. The final step to produce the 1 mm sampling interval is a 1 mm rotation of the detector ring [13].

2. Scintillator Dimensions

From the above discussion we see that for proper reconstruction of positron sources, the detector width W should not exceed 2 mm. Since most of the detector "width" is introduced through the azimuthal dimension W of the scintillator (Fig. 1), we choose W in Fig. 1 to be 2 mm. The radial

dimension L of the scintillator contributes to the scintillator "width" for sources not on the detector ring axis. Assuming that the radioactive source region extends no more than 10 cm from the ring axis and that the scintillator ring radius is 50 cm, a value of $L = (40/10)W$, or 8 mm, will not add significantly to the effective width of the detector (7).

The axial dimension of the scintillators would also be 4 mm to provide the same resolution in the axial direction.

B. THE NECESSITY FOR LIGHT CODING

Assuming a radius of 40 cm for the detector ring and a 2 mm width for each detector, the total number of detectors in the ring is about 1,250. One detector layer might be sufficient in each ring for BGO detectors, since the 8 mm thickness represents 8.8 mean-free-paths for 511 keV gamma rays, and hence a 55% detection efficiency (although only a 30% coincidence detection efficiency). In the present design there are 10 separate detector rings (Fig. 1), so that the total number of detectors will be $10 \times 1{,}250 = 12{,}500$. (The 10 rings of detectors are desirable to recover the detection efficiency lost by using a camera with improved resolution.) If a photomultiplier were coupled to each detector, the photomultiplier cost alone would then be $1.25 million, assuming a cost of $100 for each photomultiplier. Such a cost is very high, if not unrealistic. Clearly, there is a cost barrier for reducing detector size down to 2 mm if scintillators are to be coupled directly to photomultipliers.

This barrier can be removed by using coding methods for transmitting the light from each scintillator to two or more photomultipliers (7,9,14). With such light coding, the number of photomultipliers is greatly reduced. For example, a system of 12 rings with detectors that have a 2.4 mm effective width has been designed (7) which uses 200 photomultipliers (320,000 instead of the 12,500 directly-coupled photomultipliers above ($1.25 million). (Even though the scintillator widths are 2 mm at the inner circumference, they are 3 mm at the outer circumference, and the mean width of the scintillators turns out to be 2.4 mm.) We conclude, thus, that further progress in achieving better spatial resolution requires coding for the transmission of light from scintillators to photomultipliers.

C. A SCINTILLATOR FIGURE-OF-MERIT

We now consider the various factors (efficiency, background suppression) which determine the effectiveness of a ring tomograph using light coding. The scintillator properties (amount of light emitted, light decay constant) which affect this tomograph effectiveness are then combined to give a figure-of-merit quantity for the scintillator.

1. Light Losses Introduced by Light Coding.

First, there is a division of scintillation light among the light pipes connecting each scintillator to several photomultipliers. Second, only a small fraction of the light is accepted by the light pipes which transmit the light to the photomultipliers. While servicing the many small scintillators (Fig. 1), it is almost mandatory that coated optical fibers be used to protect the optical surfaces and to prevent cross-talk between fibers. Such fibers accept light over only about 6% of the 4π solid angle (15). In addition to other small losses, there is an attenuation of about 3 times in transmission through a typical 1-m-long optical fiber. Thus the amount of light at the photomultipliers is reduced a factor of 2 (number of photomultipliers) $\times$ 0.06 (solid angle factor) $\times$ 3 (light attenuation in fiber) = 100, when using a coding system. This factor-of-100 loss in number of photons has a significant impact on the choice of scintillator to be used.

2. Pulse Height Considerations

One effect of the reduction of the amount of light at the photomultiplier by a factor of 100 is that the fractional width of a "photopeak" in a pulse height distribution is increased by $(100)^{1/2} = 10$. For BGO, the only scintillator producing a significant photopeak for 511 keV annihilation gamma rays stopped in small scintillators, the fractional peak width will increase a factor of 10 from its usual 17% value (16); the photopeak is washed out, therefore, and the pulse height distribution becomes a featureless continuum.

If pulse height spectra for all scintillators using optical fibers are, thus, simply continua, the main effect of a light transmission loss is to increase the fraction of the lower end of the continuum that does not produce even one photoelectron at the photomultiplier, so that the scintillation is not even recorded. Thus the number of photoelectrons n_e produced at the upper end of the pulse height continuum is associated with the scintillation detection efficiency and should be included in the figure-of-merit.

3. Time Resolution Considerations

The amount of scintillation light, however, is not the only factor that needs to be considered. The number of accidental coincidence events is proportional to τ, the width of the electronics logic pulses. This width can be no smaller than the time jitter Δt which occurs when the logic pulses are produced from the scintillation pulses. We now show that the number of accidental coincidence events is a significant factor in a positron tomograph ring, so that the magnitude of the time jitter Δt is important.

The Donner group has measured (17) the ratio of accidental events, C_a, to true coincidence events, C_t, to be

$$C_a/C_t = 1,400/4,000 = 35\%$$

for a pulse resolving time $\tau = 20$ nsec and an activity of 300 μCi/axial cm. [This measurement agrees, within a factor of 2, with their design calculation (9).] Now the time jitter Δt of the electronic signal is

$$\Delta t = k(\tau/n_s^{1/2}) \tag{1}$$

where k is a constant, τ is the light decay constant for the scintillator, and n_s is the number of photoelectrons at the photomultiplier photocathode. If, because of coding, n_s is reduced a factor of 100 then, according to Eq. 1, the time jitter Δt is increased a factor of 10. Consequently, the accidental coincidence rate will increase from 35% to 3.5 times the true coincidence rate. The time jitter must, therefore, be kept small and the factor $n_s^{1/2}/\tau$ from Eq. 1 should be included in the figure-of-merit.

C. A Scintillator Figure-of-Merit

A figure-of-merit might then be defined as the product of n_s (section 2) and $n_s^{1/2}/\tau$ (section 3 above). At this point, however, it is not clear whether the two factors are of equal importance, and also, such a figure-of-merit has no physical significance. If, however, we use $n_s^{1/2}$ for the pulse height factor of section 2 instead of n_s, then the figure-of-merit becomes

$$\text{Figure-of-merit} = n_s/\tau.$$

Since, for a given detector system, the number of photoelectrons n_s is proportional to the number of photons emitted by the scintillator, we can also express this figure-of-merit for the scintillator as

$$\text{Figure-of-merit} = \frac{\text{Number of photons emitted}}{\text{Decay constant for emission}}, \tag{2a}$$

or equivalently,

$$\text{Figure-of-merit} = \text{rate of photon emission}. \tag{2b}$$

This figure-of-merit is, then, a simple physical property of any scintillator.

D. COMPARISON OF SCINTILLATORS

In this section we compare several scintillators using the figure-of-merit just developed (Eq. 2a). The comparison is exhibited in Table 1. The plastic scintillator, NE102, has a figure-of-merit that is 480 times larger than the figure of merit for BGO and 32 times larger than the figure-of-merit for NaI(Tl). On the basis of figure-of-merit alone, NE102 is the preferable scintillator.

However, other scintillator characteristics could conceivably eliminate NE102 from consideration. Remarkably, the evaluation of the other characteristics serves to eliminate the other scintillators instead. First, because of its hygroscopic nature, NaI(Tl) must be hermetically sealed, and successful sealing is difficult for large arrays. In fact, partly because of difficulties in packaging the many small scintillators, the NaI(Tl) scintillators in the Donner tomograph have been replaced by BGO (3).

A second factor is the ease of machining large complex scintillator arrays; here, a plastic scintillator such as NE102 is much to be preferred to either NaI(Tl) or BGO. Third, the cost of plastic scintillators is very much less than the cost of either of the other scintillators. And finally, because the decay constant τ is some 100 times smaller for NE102, the dead time between the processing of events will also be decreased by this factor.

On these grounds, then, a plastic scintillator such as NE102, appears to be the choice for use in positron tomographs using light coding systems.

E. ANSWERS TO POSSIBLE OBJECTIONS

1. Absence of Pulse Height Discrimination

One of the main arguments presented for using a BGO scintillator (1) is that the pulse height discriminator could be set below the large photopeak to discriminate against gamma rays that have been scattered in the body of the patient. However, most of such gamma rays are scattered in the forward

TABLE 1. *Figure-of-merit for various scintillators*

Scintillator	τ (nsec)	n_s (relative)	Figure-of-merit (relative)
Bismuth germanate	300[a]	0.08[a]	1
NaI(Tl)	250[b]	1.0	15
NE102	2.4[c]	0.31[b,c]	480

[a] Ref. 15.
[b] Ref. 24.
[c] Ref. 25.

direction and so have energies near the primary energy. Thus it is difficult to discriminate against these effectively by pulse height selection (17). Furthermore, as discussed previously, the use of a light coding system reduces the pulse height resolution so much that the photopeak in BGO is eliminated.

We now show that unwanted coincidence events are reduced sufficiently in tomographs with improved resolution so that detectors without pulse height discrimination can be used.

a. Accidental Coincidence Events

When compared to the true coincidence events, the number of accidental coincidence events scales as $I(S/T)^2$, where I is the coincidence resolving time and S and T_0 are defined in Fig. 1 (9). ($T = T_0 + \bar{r}$, where $\bar{r}$ is the mean penetration depth of the gamma rays in the detector ring.) For a tomograph designed for 2.4 mm resolution (7), the use of this scaling factor combined with the measurement of accidental coincidence events with the Donner tomograph shows that the accidental coincidences will be only 1% of the true coincidences for the 2.4 mm tomograph (Appendix A). For better resolution, S^2 becomes smaller, while T^2 is unchanged, so that the fraction of accidental events will be even smaller.

b. Scattered Coincidence Events

These events occur when one (or both) of the pair of annihilation gamma rays is scattered before being detected. The number of these events scales as S/T compared to the number of true events (9). Use of Donner tomograph data and the scaling laws indicates that these events, for the 2.4 mm tomograph (7), will contribute a background of 10% (Appendix A). Thus the largest background spectrum comes from these events. It should be noted, though, that the events will be distributed randomly across the reconstructed image; thus if the radioactive source pattern is localized, this background will be reduced below the 10% value. Furthermore, because of the S/T scaling factor, this source of background will also decrease as the resolution is improved.

2. Gamma Ray Detection Efficiency of Plastic Scintillators

The mean-free-path λ for a 511 keV gamma ray in the plastic scintillator NE102 is about 10 cm, in contrast to 1 cm for BGO. However, the thickness of the detector ring in Fig. 1 can be made as large as desired by adding layers of detectors. The practical limitation to increasing the ring thickness is the cost of providing enough optical fibers to collect the light from the ring, since the cost of the plastic scintillators is negligible. In one practical camera design (7), the detector thickness is 16 cm, or 1.6λ. The detector efficiency, then, is 80% with a coincidence efficiency of 64%.

3. Light Collection from the Scintillators

To collect the light from the scintillators, the many small rectangular scintillators in the detector ring are separated from each other by thin layers of semitransparent material of somewhat lower index of refraction (8). Light in any scintillator is then transmitted by internal reflection through neighboring scintillators in the r (radial) and θ (azimuthal) directions (see Fig. 1). Thus the optical fibers on the outer circumference of the ring transmit the θ and z (axial) addresses for a scintillation. To obtain the r-address, the light traveling through the ring in the θ-direction is collected at the ends of each of the four ring segments by mirrors.

4. Cross-Talk Between Scintillators

Since all of the gamma rays interact by Compton scattering with the scintillators in the detector rings, and since the mean-free-path λ of the gamma rays is about 10 cm, one might expect that a large fraction of the gamma rays would interact with more than one scintillator. Surprisingly, it is just the large value of λ which inhibits such multiple interactions.

The fraction of the gamma rays undergoing a second scattering within a detector ring is approximately

$$\text{Fraction rescattered within ring} = S/2\lambda, \quad (3)$$

where S is the axial dimension of the ring and λ is the mean-free-path of the gamma ray in the scintillation detector. For a plastic detector, $\lambda = 10$ cm, while for the camera under discussion, $S = 4$ mm. Thus

$$\text{Fraction rescattered within ring} = 0.4/20 = 2\%. \quad (4)$$

A more accurate calculation gives a value of about 5%.

For scattering into other detector rings, the fraction rescattered is given approximately

$$\text{Fraction rescattered in other rings} = \lambda_s/\lambda, \quad (5)$$

where λ_s is the mean-free-path for the gamma ray in the lead shield between rings. For gamma rays of energy somewhat below 511 keV, $\lambda_s = 3$ mm, while again, $\lambda = 10$ cm for the scintillator. Thus the fraction rescattered in other rings is

$$\text{Fraction rescattered in other rings} = 0.3/10 = 3\% \quad (6)$$

The fractions given Eqs. 4 and 5 are not only small, but the events they represent can be rejected by electronic means. Thus the effect of the cross-talk, or rescattering, is to reduce the ring detection efficiency by about $\frac{1}{3} + \frac{1}{3} = 13\%$. Furthermore, the SSP contribution is proportional to S, as it will decrease when thinner detector rings are used.

It might be noted here that cross-talk is a much more serious problem for BGO scintillators. For small BGO detectors, a large fraction of the scattered gamma rays leave the detector so that Eqs. 3 and 5 can be used to give rough estimates. Since the fractions for both equations are inversely proportional to λ, the mean-free-path of the scattered gamma rays, the fraction of the gamma rays rescattered will be some 10 times greater for BGO than for NE102.

5. Insufficient Light Transmission

Previously it was shown that only about 1% of the scintillation light is transmitted to the photomultipliers when using a light coding system. One might think that there would not be enough light left to produce photoelectrons at the photomultipliers, so that the gamma ray detection efficiency would be seriously reduced. A brief calculation in Appendix B shows that an efficiency of 78% can be expected for recording a stopped gamma ray. One reason for the high efficiency is that the pulse height discriminators can be set low enough to detect pulses produced by single photoelectrons. The random pulses produced by thermal noise in the photomultipliers are completely rejected by the many-fold coincidence requirement associated with a coding system.

6. Cost of a Coding System

While a tomograph using a coding system can use fewer photomultipliers than a system with photomultipliers coupled to each scintillator, the cost of the optical fibers and the assembling of the coding system itself must be included as part of the overall expense. For the tomograph with 10 rings of 2.4-mm-wide detectors that has been designed (7), the costs are estimated to be as follows:

200 photomultipliers @ $100	$ 20,000
250,000 fibers @ 25¢ each	37,500
Fiber assembly @ 10.5 man-year	85,000
Total cost	$142,000

This cost is to be compared to the $1,250 million amount calculated earlier for photomultipliers coupled to individual scintillators. Also, this cost is not a dominating factor in the total cost of a complete tomograph system, which also includes a mechanical assembly, a computer, and a display and storage capability.

F. LIMITATIONS ON SPATIAL RESOLUTION INTRODUCED BY PHOTON STATISTICS

It has often been noted that images produced by tomographic rings are particularly susceptible to degradation because of statistical effects. We wish to show here that a tomograph with 2.4 mm resolution can be designed (7) to produce images with the same statistical quality as that of the 6 mm (design) resolution Donner tomograph (3).

1. Statistics for Single-Ring Tomographs

It is well known that for a single detector ring,

$$T_1 = \text{constant}(\sigma/a)^2 S^2 l, \qquad (7)$$

where T_1 is the data collection time, σ is the standard deviation, and a is the mean number of events in a pixel, S is the axial dimension of the detector ring, and l is the pixel dimension in the plane of the detector ring. Suppose now, that we select another tomograph with S and l reduced a factor of m in magnitude. Then, if (σ/a) is kept constant, the time T_1 will increase by the factor m^3. There appears, therefore, to be a steep barrier to further decreasing pixel size in ring tomographs (11).

2. Specifying Statistical Fluctuations

In this section we will show, by means of a simple (though somewhat artificial) example, that the m^3 dependence just discussed is misleading. The example will show that one of the assumptions underlying the derivation of the m^3 dependence is inappropriate. This assumption, as just stated above, is that σ/a, the fractional deviation in the mean number of events in a pixel should be kept constant as the pixel size is decreased.

Consider now the picture of a checkerboard on a photographic film. The black squares will contain many small developed silver grains, while the white squares will have no grains. Suppose next, that the pixel size chosen to view the picture is such that one pixel contains four squares, so that each pixel contains two black squares and two white squares. Then each pixel will contain the same number of grains and our image of the checkerboard will appear to be a uniform gray.

Next, let the pixel size be reduced so that one pixel contains only one square of the checkerboard. Now, the alternating pattern of the checkerboard will have become evident. If still smaller pixels are used, the sharp edges of the checkerboard squares will begin to become apparent. The effect, therefore, of using the smaller pixels to view the photographic picture is the same as the effect produced when improving the focus of a camera viewing the picture. The use of large pixels lead to a "smeared" image, while use of small pixels "sharpens" the image.

Now, the important point in this example is that *although there changes in pixel size, the number of grains in the photographic picture will not change even though the spatial resolution of the image of the picture improved.*

In particular, the spatial resolution improved as the size of the pixels decreased even though the mean number of grains per pixel decreased (since the total number of grains in the picture was unchanged).

Now, it is easily shown that if $\sigma/\bar{n}$ is to be kept constant when the pixel size is changed, then $\bar{n}$, the mean number of grains per pixel, must also be kept constant. With Poisson statistics (which apply here), $\sigma = \bar{n}^{1/2}$, so that

$$\sigma/\bar{n} = \bar{n}^{1/2}/\bar{n} = 1/\bar{n}^{1/2} \tag{8}$$

Thus, a constant $\sigma/\bar{n}$ requires a constant $\bar{n}$.

But in our checkerboard example above, $\bar{n}$ was not constant, but rather decreased with reduced pixel size, so that $\sigma/\bar{n}$ increased. Thus the assumption of a near exact $\sigma/\bar{n}$ is too stringent, and the w^3 dependence derived from this assumption is inappropriate.

Nevertheless, there clearly is a pixel size below which little is to be gained in image quality. This size would be dependent on the number of blackened grains in the picture. Certainly, the size should not be so small that only a small fraction of the pixels have even one blackened grain. Yet, if the picture were that of a linear object, one could imagine that only every fourth pixel or so along the line might need a grain for the line to be visible to the eye. For example, when a bar chart is viewed, the bars are visible even when individual pixels do not have grains in them (19).

We are led, therefore, to the concept of an assemblage of pixels (such as those pixels defining a set of parallel bars). The assemblage, which is viewed as a unit by the human eye, is the region which must have a certain number of blackened grains to be visible. The distribution of the grains within the assemblage does always be observed better when smaller pixels are used until the pixel size is reduced below that of the resolution of the picture itself. For nonlinear sources, the minimum pixel size would be 1 mm to provide the sampling necessary for a positron line source (see section A.1).

The linear size of the assemblage of pixels which the eye views as a single unit is probably in the range of a centimeter or so. This size is a very subjective quantity, depending on the character of the image being observed. It is this assemblage which must have a minimum number of events.

Summarizing, then, the statistical criteria for the number of events required should be applied to an assemblage of pixels which includes the region of interest (with linear size in the range of a few centimeters). This assemblage of pixels will contain, then, smaller pixels which should be as small as 1 mm on a side when positron sources are being viewed.

9. The Statistical Penalty for Ring Tomographs

We now determine quantitatively how the statistical properties of the image of a positron tomograph are affected by pixel size. We begin by extending the analysis of the previous subsection to three dimensions and then incorporate the result into a statistical evaluation of the tomograph itself.

For a region of constant exposure on a photographic film, the number n of blackened grains in a pixel with dimension $l \times l$ is proportional to l^2. Thus $(\sigma/\bar{n})^2 = l^4/\bar{n}^2 = 1/\bar{n}$ will very intimately as the area l^2. If we now extend the pixel into the third (axial) dimension, $(\sigma/\bar{n})^2$ will be inversely proportional to the volume l^2S, where S is the third pixel dimension. We should therefore expect that

$$(\sigma/\bar{n})^2 = \text{Constant}/l^2S \tag{9}$$

when the pixel volume is l^2S and the number of events in a three dimensional "picture" is kept fixed, i.e., the statistical quality of the image is unchanged.

We now substitute Eq. 9 into Eq. 7 to obtain

$$T_s = \text{constant}/l^2S \tag{10}$$

Consequently, if the magnitudes of l and S are each reduced a factor of m, then the data acquisition time T_s must be increased a factor of m^2 to maintain the statistical quality of the image. Thus the use of a ring tomograph introduces a statistical penalty factor of m^2 when the pixel dimensions of the reconstructed image are each reduced by a factor m.

This m^2 dependence has been obtained here using plausibility arguments; it has also been derived in detail by the author, the result being given by

$$\frac{\Delta T/\Delta L_d}{\Delta T'/\Delta L_d'} = \frac{L_d'S'^2}{L_dS^2} = m^2/q, \tag{11}$$

Here, we are comparing the time to obtain data per unit cm $(\Delta T/\Delta L_d)$ for two tomographs. One tomograph produces pixels of size $l \times l \times S$ and the other, pixels of size $l' \times l' \times S'$, where $l' = ml$ and $S' = mS$. The parameter q is simply the ratio of the lengths of the tomographs, $q = L_d/L_d'$. The statistical fluctuations are the same for each tomograph for the same pixel size ($l' \times l' \times S'$).

4. Elimination of the Statistical Penalty

By increasing the axial length of the tomograph (increasing q), it is possible, according to Eq. 11, to keep $\Delta T/\Delta L_d$ from becoming larger than $\Delta T'/\Delta L_d'$ even though the pixel size is reduced (or increased). We show this relationship specifically by comparing the Donner tomograph (17) to the tomograph that has been designed (7). For the single-ring Donner tomograph, l' (detector opening) = 1.0 cm and S' = 1.0 cm, while $L_d' = 2S' = 2.0$ cm. For the designed 10 ring tomograph (7), we have $l = 0.45$ cm, $S = 0.45$ cm, $L_d = 10 \times 2S = 9.0$ cm. Thus from Eq. 11,

$$\frac{\Delta T/\Delta L_d}{\Delta T'/\Delta L_d'} = \frac{2.0}{9.0} \times \frac{1.0}{0.45} \times \frac{1.0}{0.45} = 0.9 \tag{12}$$

This time, then, to take data for the ten-ring tomograph is somewhat less than that for the Donner single-ring tomograph even though the spatial resolution is $1.0/0.45 = 2.1$ times better. It should be realized, however, that the time for a given single also is 9 times as long.

G. ABSOLUTE DETECTION RATES

It has been convenient in the preceding discussion to describe the tomograph (Fig. 1) in terms of the well-documented Donner tomograph (2,3,9,17, 20,21). In this section we will calculate independently the statistical quality of the images recon-

structed by a tomograph (Fig. 1) using 10 detector rings of plastic scintillators (7). Where convenient, we will continue to use Donner laboratory parameters (9).

First, we calculate the sensitivity of the tomograph by evaluating C_d/ρ. Here C_d is the counting rate for a single detector ring and ρ is the radioactivity density in μCi/axial cm. We have (7) S = 0.48 cm, the detector radius c = 38.6 cm, and the detection efficiency ϵ = (0.80 × (0.78) × (0.87) = 54%. The 0.80 factor is the fraction of the 511 keV gamma rays interacting with the ring detectors (7), the 0.78 factor is the efficiency for detecting scintillations (Appendix B), and the 0.87 factor introduces the effect of rejecting events because of "cross-talk" between detectors. We also have (9) e = $\exp(-\mu L)$ = 0.135, where μ = 0.10 (water) is the gamma ray absorption coefficient, and L = 20 cm is the diameter of the body containing the gamma ray source. The sensitivity for one detector ring is found to be C_d/ρ = 2.1 events/sec/(μCi/axial cm), and for the tomograph (10 slices),

$$\text{Sensitivity} = 21 \text{ events/sec/(}\mu\text{Ci/axial cm)} \quad (13)$$

This value is comparable to that of the Donner tomograph when S (the axial dimension) is 1.3 cm (3).

The time to take data can be written as (21)

$$T = \frac{17.6\{F + (1 - F)/C\}^{1/2}}{(\sigma_A/n_A)^2 V l} \quad (14)$$

Here σ_A is the standard deviation and n_A is the mean of the number of events in an "assembled" pixel of volume V. The "assembled" pixel is the volume containing the object of interest. An expression has been derived for σ_A/n_A,

$$\sigma_A/n_A = 0.20(1 - 1/C), \quad (15)$$

where $C = n/n_b$. Here, n is the mean number of events in the "target" (high radioactivity) pixels, while n_b is the mean number of "background" events in the remaining pixels. The basis for the expression for σ_A/n_A in Eq. 15 is that the probability is less than unity that the number of events in *any* one of the "target" pixels will be as small as n_b, the mean number of events in the background pixels.

It is interesting that for the case of no background events ($1/C$ = 0), Eq. 15 gives a value for 20% for σ_A/n_A, which is a value that has been used in the literature (21).

Inserting Eq. 15 into Eq. 14, we obtain

$$T = 440\{F + (1 - F)/C\}^{1/2}(1 - 1/C)^2 V l \quad (16)$$

The remaining parameters in Eq. 16 have the following meaning. The "target" pixels cover a fraction F of all the pixels in each transaxial plane, while l is the pixel dimension (sampling interval) in the transaxial planes. Equation 16 expresses the time in seconds to scan an axial distance of 9.6 cm for a total volume of 3,000 cm³.

We next use Eq. 16 to find T for several different distributions of radioactivity. We consider small regions where the effectiveness of the good spatial resolution of the tomograph would be most apparent.

1. Small, Radioactively Smooth "Dark" Objects in a Uniform "Bright" Background

For this situation, F, the fraction of the transaxial area that is "bright" is arbitrarily unity. Thus

$$T = 440V(1 - 1/C)^2 l. \quad (17)$$

a. A 1 cm³ Spherical Shape.

Here we can select a sampling interval of l = 0.96 cm. (The 0.96 cm interval is obtained by electronically combining the 0.24 cm detectors in groups of four.) We then find for T in Eq. 14, with V = 1 cm³:

$$T = 9.4 \text{ minutes } (C = 10), \quad (18a)$$
$$T = 17.2 \text{ minutes } (C = 5). \quad (18b)$$

b. A 10-cm-long Curved Line Having a 0.5 cm Diameter

Here we must use l = 0.48 cm, while the volume is 2.0 cm³. Since l is halved while V is doubled compared to the preceding case, the times are the same as those in Eqs. 18.

2. Small, Radioactively Smooth "Bright" Objects in a Uniform "Dark" Background

In this case, $F << 1$, and Eq. 16 becomes

$$T = 440\{1/C\}^{1/2}(1 - 1/C)^2 V l. \quad (19)$$

a. A 1 cm³ Spherical Shape with Smoothly Varying Density

With l = 0.96 cm, we find

$$T = 18 \text{ sec } (C = 10), \quad (20a)$$
$$T = 3.3 \text{ min } (C = 5). \quad (20b)$$

These times would be doubled if 0.48 cm pixels were used.

b. A 10-cm-long Curved Line Having a 0.50 cm Diameter

Here the pixel size must be reduced from 0.96 to 0.48 cm, since the volume has been doubled but the pixel size has been reduced from 0.96 cm, the times are the same as those in Eqs. 20.

3. One-Tenth of the Volume is "Bright" in a Uniform "Dark" Background

To define the edge of the volume we select l = 0.24 cm. We select C = 4 so that the conditions are similar to

tissue used as an example (for dynamic studies) in the literature (21). Then, Eq. 16 gives

$$T = 10^3 V = 0.053 \text{ sec}, \quad (21)$$

since $V = 3{,}000 \text{ cm}^3/10 = 300 \text{ cm}^3$. This time is so small because of the large value of the volume of the object (equivalent to an 8-cm diameter sphere). Such a short time is probably unrealistic because we have assumed that the visual process will integrate the large volume into a coherent pattern. We also have the problem of displaying (and visualizing) a large object in three dimensions.

In conclusion, we can state that images of objects of interesting size can be obtained in reasonable times. These results are based on the plausible assumption that the objects will be integrated into units by the visual process. The whole question of displaying three-dimensional images has been avoided.

II. SUMMARY

It has been shown that because of photomultiplier noise, light coding systems cannot be used with tomographic ring cameras having spatial resolutions of 2 mm. Consequently, because of the light loss introduced by coding, the plastic, NE102, is a much better choice for a scintillator than BGO or NaI(Tl).

It was then shown that (a) the absence of pulse height resolution with NE102 does not lead to serious background problems; (b) a detector ring of plastic scintillators can have a detector efficiency of 80% (or better); (c) light can be extracted from a closely packed array of scintillation detectors; (d) the cross-talk between detectors is about 13%; (e) enough light can be transmitted through the coding system to yield a 78% efficiency for detecting scintillations, so that the total detection efficiency for each gamma ray is $0.80 \times (1 - 0.13) \times 0.78 = 54\%$; and (f) the cost of a coding system is only about 10% of the cost of coupling photomultipliers directly to detectors for a tomograph with 2.4-mm-wide detectors.

Next it was shown that the data acquisition time increases only as n^2 when pixel dimensions are reduced by a factor of n. Furthermore, this increase in statistical fluctuation can be somewhat compensated for by extending the axial length of a multi-ring tomograph. Because of these considerations, it is shown that a designed multi-ring tomograph with 0.24 cm resolution has a detection sensitivity comparable to that of the Donner 280-detector tomograph.

There appears, therefore, to be no serious barrier to producing tomographic cameras with spatial resolutions of 2 mm or better.

ACKNOWLEDGMENTS

The authors would like to thank Drs. T. F. Hayniz and M. F. Jahns for helpful discussions.

APPENDIX A

Here we calculate the background introduced by (a) accidental coincidence events and (b) true coincidence events from scattered gamma rays. The calculations are made by taking experimental data obtained with the Donner tomograph (17) and by using the theoretical scaling laws (9) to obtain the background for a tomograph that has been designed with 2.4 mm resolution (7). The reliability of these scaling laws has been confirmed by Donner measurements (17).

1. Accidental Coincidence Events

The Donner group measured the accidental counting rate C_a to be 35% of the true coincidence rate C_c using a logic pulse width t of 20 nsec. The ratio C_a/C_c scales as $t(S/T)^2$. For the Donner tomograph, $S = 2$ cm and $T = 20$ cm, while for the 2.4 mm tomograph, $t = 5$ nsec (the decay time for the NE102 scintillator is 2.4 nsec), $S = 4.8$ mm, and $T = 13.6$ cm. Thus C_a/C_c for the 2.4 mm tomograph will be

$$\frac{C_a}{C_c} = \left[\frac{5}{20}\right] \times \left[\frac{0.48}{2.0}\right]^2 \times \left[\frac{20}{13.6}\right]^2 \times 35\% = 1\%.$$

2. Scattered Coincidence Events

The Donner group measured the scattered coincidence rate C_s to be 29% of the true coincidence rate C_c. The ratio C_s/C_c scales as S/T, so that for the 2.4 mm tomograph,

$$\frac{C_s}{C_c} = \left[\frac{0.48}{2.0}\right] \times \left[\frac{20}{13.6}\right] \times 29\% = 10\%.$$

APPENDIX B: NUMBER OF PHOTOELECTRONS PRODUCED

According to Hartman (22), the energy in the light photons from NaI(Tl) is about 15% of the energy deposited in the NaI(Tl) by an energetic charged particle. For the plastic NE102, the efficiency is 31% of this value (23,24), which yields a light conversion efficiency of 4.65%. The blue scintillation light photon energy is 3.1 eV. This light is then converted to photoelectrons at the photomultiplier with an efficiency of 22% (25). There is also an 80% efficiency for collecting light from the multiple scintillators (8). Inserting the factor of 100 light loss introduced by the optical fibers (tabulated in the section on light losses), the maximum number of photoelectrons produced by a 511 keV gamma ray is

$$\text{Number of photoelectrons (511 keV)} = \frac{511 \times 10^3 \times 0.22 \times 0.046 \times 0.80}{3.1 \times 100} = 13.$$

However, the pulse height spectrum in a plastic scintillator extends from zero to two-thirds of the height associated with the total energy of 511 keV. Thus to a rough approximation, the pulse height spectrum can be considered to be a constant in amplitude from zero to 9 photoelectrons.

For the coding system used in the tomograph design (7), scintillation light is collected at two surfaces and transmitted to 5 photomultipliers in coincidence. The effect of this coincidence requirement is to produce a coincidence spectrum extending from 2 to 9 photoelectrons. Thus 7/9 of the spectrum survives the coincidence, and the efficiency for detecting a scintillation is 78% for each gamma ray detected.

REFERENCES

1. Cho ZH, Farukhi MR: Bismuth germanate as a potential scintillation detector in positron cameras. *J Nucl Med* 18:840–844, 1977
2. Derenzo SE: Positron ring cameras for emission-computed tomography. *IEEE Trans Nucl Sci* 24:881–885, 1977
3. Derenzo SE, Budinger TF, Cahoon JL, Greenberg WL, Huesman RH, Vuletich T: The Donner 280-crystal high resolution positron tomograph. *IEEE Trans Nucl Sci* 26: 2790–2793, 1979
4. Thompson CJ, Meyer E, Yamamoto YL: Positome II: A high efficiency P.E.T. device for dynamic studies. *J Comput Assist Tomogr* 2:650–651, 1978
5. Cho ZH, Nalcioglu O, Farukhi MR: Analysis of a cylindrical hybrid positron camera with bismuth germanate (BGO) scintillation crystals. *IEEE Trans Nucl Sci* 25: 952–963, 1978
6. Ter-Pogossian MM, Mullani NA, Hood JT, Higgins CS, Ficke DC: Design considerations for a positron emission transverse tomograph (PETT V) for imaging of the brain. *J Comput Assist Tomogr* 2:539–544, 1978
7. McIntyre JA: Design features of a positron tomograph with 3.4 mm resolution. *IEEE Trans Nucl Sci* (in press)
8. McIntyre JA: A three-dimensional position-sensitive gamma ray detection system. *Nucl Instr Methods* (in press)
9. Derenzo SE, Zaklad H, Budinger TF: Analytical study of a high-resolution positron ring detector system for transaxial reconstruction tomography. *J Nucl Med* 16:1166–1173, 1975
10. Phelps ME, Hoffman EJ, Huang SC, Ter-Pogossian MM: Effect of positron range on spatial resolution. *J Nucl Med* 16:649–652, 1975
11. Muehllehner G: Resolution limit of positron cameras. *J Nucl Med* 17:757, 1976
12. Brooks RA, Sank VJ, Talbert AJ, Di Chiro G: Sampling requirements and detector motion for positron emission tomography. *IEEE Trans Nucl Sci* 26:2760–2763, 1979
13. Cho ZH, Eriksson L, Chan JK: Reconstruction tomography in diagnostic radiology and nuclear medicine. Baltimore, University Park Press, 1977
14. McIntyre JA, Snyder DP: Radiation image amplifier and display comprising a fiber optic matrix for detecting and coding the radiation image pattern. US Patent 3,652,855, 1972
15. Designing with CROFON light guides. Wilmington, Delaware, E. I. duPont de Nemours & Co.
16. Nestor OH, Huang CY: Bismuth germanate: A high-Z gamma ray and charged-particle detector. *IEEE Trans Nucl Sci* 22:68–71, 1975
17. Derenzo SE, Budinger TF, Cahoon JL, Huesman RH, Jackson HG: High resolution computed tomography of positron emitters. *IEEE Trans Nucl Sci* 24:544–558, 1977
18. Hoffman EJ, Phelps ME: An analysis of some of the physical aspects of positron transaxial tomography. *Comput Biol Med* 6:345–360, 1976
19. Rose A: Vision, Human and Electronic. New York, Plenum Press, 1974, Chap 1
20. Budinger TF, Derenzo SE, Gullberg GT, Greenberg WL, Huesman RH: Emission computer assisted tomography with single-photon and positron annihilation photon emitters. *J Comput Assist Tomogr* 1:131–145, 1977
21. Budinger TF, Derenzo SE, Greenberg WL, Gullberg GT, Huesman RH: Quantitative potentials of dynamic emission computed tomography. *J Nucl Med* 19:309–311, 1978
22. Harshaw Scintillation Phosphors. Solon, Ohio, Harshaw Chemical Co., 1975, p 4
23. Swank RK: Characteristics of scintillators. In: Annual Reviews of Nuclear Science. Stanford, California, Annual Reviews, Inc., 1954, p 137
24. Table of Physical Constants of Scintillators. San Carlos, California, Nuclear Enterprises
25. Data Sheet for 4516 Photomultiplier. Harrison, New Jersey, RCA, 1967